PAPER • OPEN ACCESS

Manipulating and trapping skyrmions by magnetic field gradients

New Journal of Physics
The open access journal at the forefront of physics

Deutsche Physikalische Gesellschaft DPG
IOP Institute of Physics

Published in partnership with: Deutsche Physikalische Gesellschaft and the Institute of Physics

OPEN ACCESS

RECEIVED
29 March 2017

REVISED
24 May 2017

ACCEPTED FOR PUBLICATION
8 June 2017

PUBLISHED
8 August 2017

PAPER

Manipulating and trapping skyrmions by magnetic field gradients

Chengjie Wang[1], **Dun Xiao**[1], **Xing Chen**[1], **Yan Zhou**[2] **and Yaowen Liu**[1]

[1] Shanghai Key Laboratory of Special Artificial Microstructure Materials and Technology, School of Physics Science and Engineering, Tongji University, Shanghai 200092, People's Republic of China
[2] School of Science and Engineering, The Chinese University of Hong Kong, Shenzhen, 518172, People's Republic of China

E-mail: yaowen@tongji.edu.cn

Keywords: magnetic skyrmion, soliton dynamics, micromagnetics

Supplementary material for this article is available online

Abstract

The effective manipulation of skyrmion motion introduces the technologically relevant possibility of skyrmion-based spintronics. Here we show how a magnetic skyrmion can be captured by a radially spatial gradient of the magnetic field. A theoretical model governed by the Thiele equation is employed to study the skyrmion motion. The analytical predictions are compared to micromagnetic simulations based on the Landau–Lifshitz–Gilbert equation, showing that the dynamic behavior of skyrmions strongly depends on the gradient strength of magnetic fields as well as the radius of the skyrmion and the Gilbert damping factor. Moreover, we find that the skyrmions can also be dragged by a moving magnetic tip.

1. Introduction

Magnetic skyrmions, topologically stable magnetization textures with particle-like properties, have recently attracted great attention. The magnetic skyrmions are fundamental magnetic structures that hold promise for applications in spintronic devices; for example, functional skyrmion racetrack memory [1–7]. In comparison with magnetic vortices [8–10] or bubbles [11], one of the most interesting characteristics of skyrmions is the topological protection, which maintains the robustness with respect to the perturbations and disorder [12]. Moreover, the critical currents required to move skyrmions are very small, typically a few 10^6 A m^{-2}, which is about five orders smaller than the threshold of current-induced domain wall motion [1]. To date, three different types of skyrmions have been reported in materials with perpendicular magnetic anisotropy (PMA): bubble skyrmions [13, 14], nano-skyrmions [2, 15, 16], and dynamical skyrmions [17]. They are stabilized by different mechanisms, as follows. (i) The bubble skyrmions with a typical lateral size of the order of 1 μm are stabilized by the competition between the PMA and magnetostatics (i.e. long-range dipole-dipole interaction) [18]. (ii) The nano-skyrmions have typical dimensions of few tens of nanometers, and are stabilized by PMA and the Dzyaloshinskii–Moriya interaction (DMI) [19, 20]. (iii) The dynamical skyrmions can be stabilized by the PMA and dynamics [17], without magnetostatics or DMI.

Reliable control of skyrmion motion is of great importance and interest. Previous work has shown that the motion of skyrmions can be driven by using spin-polarized current [21–26], magnetic field gradients [27, 28], electric field gradients [29, 30], temperature gradients [27, 31, 32], magnons [33, 34], or spin waves [35]. Among these, the magnetic field gradients along the y-axis direction, as shown in figure 1(a), can induce a Hall-like motion of skyrmions, showing that in addition to the main velocity along the x-axis direction (v_x) induced by the magnetic field gradient, a slight transverse velocity can also be caused along the y-axis direction (v_y) due to the damping effect. Recently, a theoretical study on the dynamics of skyrmions driven by a magnetic field gradient has been published [36], in which the skyrmion is considered as a soliton and its dynamics is analyzed by the momentum calculation.

In this paper, we investigate the dynamics of skyrmions driven by a magnetic field gradient. The theoretical predictions are verified by micromagnetic simulations, showing how parameters such as gradient strength and

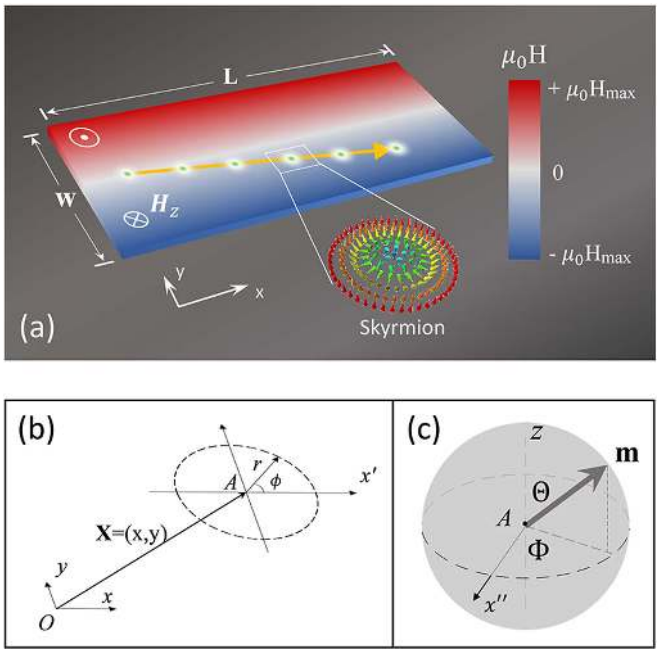

Figure 1. (a) Schematic diagram of a hedgehog (Néel-type) skyrmion motion driven by a magnetic field gradient along a nanowire thin film. The magnetic field is applied in the direction perpendicular to the film plane and its gradient strength distribution is indicated by the color bar, where the red denotes the $+z$-direction and the blue denotes the $-z$-direction. (b) Spatial coordinates (x, y) of the nanowire and the local polar coordinates (r, ϕ) of the skyrmion structure. (c) The local spherical coordinates of magnetic moment (Θ, Φ).

Gilbert damping affect the dynamical characteristics of skyrmions. Interestingly, we show that a radially gradient magnetic field can be used to trap a series of skyrmions.

2. Analytical model

As a simulation model, we consider a Néel-type skyrmion formed in the center-line of a nanowire, as shown in figure 1(a). The spin dynamics of this system can be described by the Landau–Lifshitz–Gilbert (LLG) equation [17, 37] including the DMI effect. The DMI energy density is written as $D_i[m_z(\nabla \cdot \boldsymbol{m}) - (m \cdot \nabla)m_z]$, where D_i is the interfacial DMI constant. The applied spatially dependent magnetic field at the mass center $\mathbf{X} = (X, Y)$ of the skyrmion is

$$\mathbf{H} = (0,\ 0,\ h_0 + gr\ \sin\varphi), \tag{1}$$

where (r, φ) are the local polar coordinates (see figure 1(b)), h_0 is the local magnetic field at the center, and g is the gradient parameter. Here, we consider the skyrmion as a rigid structure (without any or with very slight structure deformation). Thus the Thiele approach based on the course-grain approximation can be employed to analytically model the skyrmion dynamics [27, 35, 38–40]:

$$\mathbf{G} \times \mathbf{v} + \vec{\boldsymbol{D}}\mathbf{v} - \nabla V_{\text{grad}}(\mathbf{X}) + \mathbf{F}_{\text{edge}}(\mathbf{X}) = 0 \tag{2}$$

where $\mathbf{v} = \mathrm{d}\mathbf{X}/\mathrm{d}t$ is the instantaneous velocity of the skyrmion. $\mathbf{G}$ is the total gyromagnetic coupling vector. For the Néel skyrmion, it has a z-component only $G_Z = \int \mathrm{d}r^2 m \cdot (\partial_x m \times \partial_y m) = 4\pi W$, where W is the skyrmion number. For a single skyrmion, $W = -1$. The second term describes the dissipative process and $\vec{\mathbf{D}}$ is the dissipative tensor whose elements are given by $D = D_{xx} = D_{yy} = \alpha \int \mathrm{d}r^2 \partial_x \boldsymbol{m} \cdot \partial_y \boldsymbol{m}$ [41, 42]. The force acting on the skyrmion can be expressed as

$$F_{\text{grad}} = -\nabla V_{\text{grad}} = \int \left(\frac{\partial E}{\partial \Theta} \nabla \Theta + \frac{\partial E}{\partial \Phi} \nabla \Phi \right) \mathrm{d}r^2 \tag{3}$$

where Θ and Φ stand for the polar angle and azimuthal angle of the spin moment in the standard spherical coordinates, as shown in figure 1(c), and E is the Zeeman energy density. $\mathbf{F}_{\text{edge}}$ in equation (2) is the repulsive force generated by the boundary of the sample. In this study, we consider that the skyrmion is far away from the boundary of sample. Thus, the edge effect is ignored and $\mathbf{F}_{\text{edge}} \approx 0$.

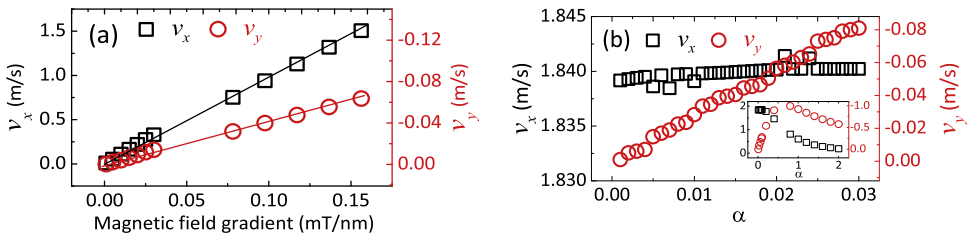

Figure 2. (a) The dependence of skyrmion motion velocity on the gradient strength of magnetic field at $\alpha = 0.03$. The hollow symbols are the simulation results. The solid lines are the analytical values from equation (4). (b) The velocity changes with the Gilbert damping α. The inset shows the virtual change of α at large scale from 0 to 2.0.

From equation (2) we can obtain an explicit solution for the skyrmion displacement driven by the magnetic field gradient:

$$\begin{pmatrix} v_x \\ v_y \end{pmatrix} = \frac{F_{\mathrm{grad},y}}{G^2 + D^2} \begin{pmatrix} -G \\ D \end{pmatrix}, \tag{4}$$

$$F_{\mathrm{grad},y} = \mathrm{g} \int_{R_{\mathrm{SK}}} \frac{\partial}{\partial y}(y m_z)\,\mathrm{d}r^2, \tag{5}$$

where $F_{\mathrm{grad},y}$ is the y-component of the driving force. The subscripted R_{SK} indicates the area of the skyrmion. Note that the displacement velocity of the skyrmion shown in equation (4) contains two components (v_{x} and v_{y}), where v_{x} is perpendicular to the field gradient and caused by the gyromagnetic force; v_{y} is parallel to the field gradient and associated with the Gilbert damping (that is, the dissipative force).

3. Simulation and results

The above theoretical predictions have been verified by micromagnetic simulations based on the LLG equation. The simulations are performed using the open-source simulation software MuMax3 [43]. We consider a ferromagnetic thin film with dimensions of $512 \times 512\ \mathrm{nm}^2$. The film thickness is 2.0 nm. The following parameters are used [35]: $M_{\mathrm{S}} = 580\ \mathrm{kA\ m^{-1}}$ (saturation magnetization), $K_1 = 800\ \mathrm{kJ\ m^{-3}}$ (magnetic anisotropy), $A_{\mathrm{ex}} = 15\ \mathrm{pJ/m}$ (exchange constant), $D_{\mathrm{i}} = 3.2\ \mathrm{mJ\ m^{-2}}$ (DMI), and $\alpha = 0.03$ (Gilbert damping). In our simulations, the sample is divided into $1024 \times 1024 \times 1$ unit cells, corresponding to a cell size of $0.5 \times 0.5 \times 2\ \mathrm{nm}^3$, which is smaller than both the Néel exchange length $\lambda_{\mathrm{Neel}} = \sqrt{2A/(\mu_0 M_{\mathrm{S}}^2)} = 8.42$ nm and the Bloch exchange length $\lambda_{\mathrm{Bloch}} = \sqrt{A/K} = 4.33$ nm. A periodic boundary condition in the x-direction is used. The total simulation time is 50 ns. The displacement of the skyrmion is characterized by the position of skyrmion center $\mathbf{X} = (X, Y)$, which can be given by the distribution of the local magnetization [11]:

$$X = \frac{\int x(1 - m_z)\,\mathrm{d}x\mathrm{d}y}{\int (1 - m_z)\,\mathrm{d}x\mathrm{d}y}, \quad Y = \frac{\int y(1 - m_z)\,\mathrm{d}x\mathrm{d}y}{\int (1 - m_z)\,\mathrm{d}x\mathrm{d}y}. \tag{6}$$

Figure 2(a) shows the simulated skyrmion velocity (v_x and v_y) as a function of the field gradients. Here the velocity is numerically calculated by $\mathbf{v} = \mathrm{d}\mathbf{X}/\mathrm{d}t$ and the gradient increases from 0 to 0.18 mT nm^{-1}. Apparently, the simulation results (symbols) agree well with the theoretical prediction of equation (4) (solid lines), showing a proportional relation between the velocity and field gradient. However, the skyrmion state will be broken if the magnetic field is too strong [14]. It can be seen in figure 2(a) that the v_{x} (perpendicular to the magnetic field gradient direction) is positive while v_{y} (along the gradient direction) is negative. v_{y} is two orders smaller than v_x when the Gilbert damping constant α is adopted to be 0.03. The influence of the Gilbert damping is shown in figure 2(b), where v_{x} (black squares) is almost invariant for the small Gilbert damping factor ($\alpha < 0.1$) while v_{y} (red circles) increases linearly with the damping factor. This feature can be explained well by equation (4), in which v_{y} is proportional to the dissipative factor D (related to the damping α) and v_{x} is independent of D. The ratio of velocity along the x- and y-directions is coincident with the Hall-effect-like angle $\tan\Theta_{\mathrm{H}} = v_{\mathrm{y}}/v_{\mathrm{x}} = -D/G$, which stands for the deflection angle [40]. However, both v_{x} and v_{y} in the inset of figure 2(b) show a nonlinear dependence when α is further increased from 0.3 to 2.0. We attribute this nonlinear decrease to the over-damping effect, which induces an inhibition contribution to the skyrmion's movement.

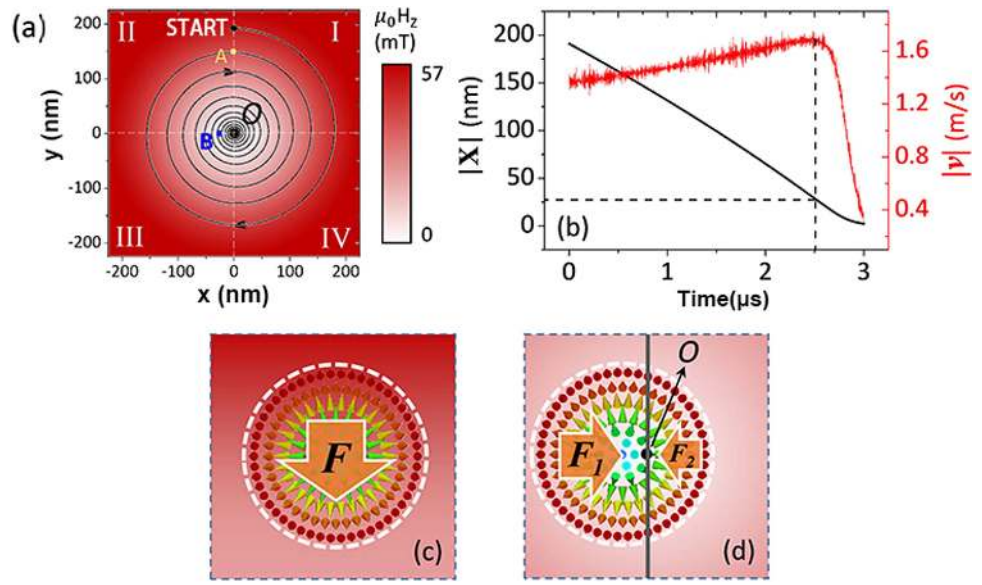

Figure 3. (a) Distribution of the gradient magnetic fields and the trajectory of skyrmion motion.The two transient states at moments 'A' and 'B' marked in (a) are shown in (c) and (d), respectively. (b) Time dependence of the skyrmion velocity (red curve) and displacement (black solid curve) apart from the sample center *O*.

3.1. Radially spatial gradient of magnetic field

The skyrmion motion triggered by the gradient magnetic fields provide a potential approach to addressing magnetic skyrmions. In the following, we will show quite an interesting dynamics: a radial direction of the magnetic field gradient can trap and capture skyrmions in a confined thin film structure. As an example, here we consider a square shaped confined structure with dimensions of $512 \times 512 \times 2$ nm^2. The discretized cell for simulations is set to be $2 \times 2 \times 2$ nm^3. In the simulations, a magnetic skyrmion is nucleated at the 'start' position marked in figure 3(a) using a local magnetic field pulse (along the $-z$-direction). After that, an inhomogeneous perpendicular magnetic field is applied along the $+z$-direction. The inhomogeneous field has a radial direction gradient with the minimum zero field at the sample center marked by a symbol '*O*' and the maximum field is ~57 mT at the boundary of the sample. Correspondingly, the radial gradient strength is 0.175 mT nm^{-1}. This is a reasonable value which can be created by a magnetic tip with typical parameters (not shown). Under the action of the magnetic field gradient, the skyrmion consequently moves toward the center of the sample along a clockwise spiral trajectory, as shown in figure 3(a).

Figure 3(b) shows the evolution of the skyrmion velocity and the displacement *d* deviated from the sample center point *O*. It is interesting to note that the skyrmion is first accelerated and then decreases rapidly after its maximum velocity obtained at $t = 2.4$ μs. This acceleration behavior can be explained from the theory based on equations (4) and (5). It is found that the radius of the skyrmion depends on the external magnetic field, which can be derived from the minimum-energy principle: [35]

$$R_{\mathrm{SK}} = \frac{D_{\mathrm{i}}\pi^2}{8\mu_0 M_{\mathrm{s}} H_{\mathrm{app}}/\pi + 2\mathrm{K}_1\pi} \tag{7}$$

where R_{SK} is the size of the skyrmion region, which increases with the decrease of magnetic field H_{app} and anisotropy K_1. This will enhance the integration value of equation (5) and further enlarge the velocity given in equation (4). As a result, the skyrmion slightly accelerates, as shown in figure 3(b). In this simulation, the gradient field is not strong enough to change the skyrmion shape.

Interestingly, the sudden decrease in velocity is observed in figure 3(b) for $t > 2.4$ μs. At this moment, the periphery of the skyrmion starts crossing the sample center 'O' point. The velocity is mainly determined by the force distribution calculated by equation (5). At the moment 'A', the skyrmion is far away from the sample center ($\mu_0 H = 0$) and the force *F* generated by the magnetic field is along the direction of the field gradient, as shown in figure 3(c). In contrast, at the moment 'B', the force F_1 generated in the left region of the solid line is pointing to the right while the force F_2 in the right region is pointing to the left, as illustrated in figure 3(d), here $F_2 < F_1$. The sum of the two forces results in a reduced driving force acting on the skyrmion particle. Consequently, the skyrmion will slow down and eventually stop at the sample center. This simulation suggests an effective method to trap or capture the skyrmions.

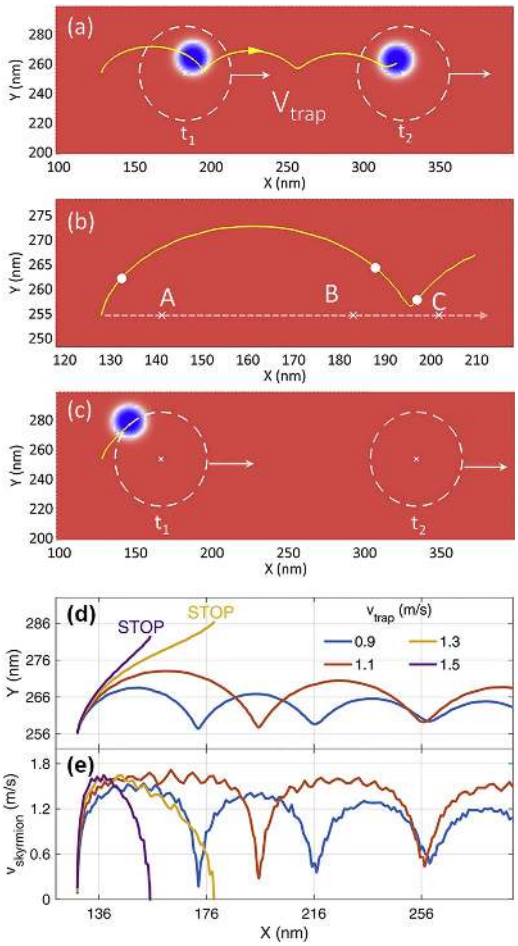

Figure 4. Skyrmion motion controlled by a moving gradient field trap along the x-direction at different constant velocities V_{trap}: (a) $V_{trap} = 1.1$ m s^{-1} and (c) $V_{trap} = 1.5$ m s^{-1}. The yellow curves indicate the trajectory of the skyrmion center. The white dotted circles indicate the active area of magnetic field trap. Two typical moments are marked by 't_1' and 't_2'. (b) The enlarged view of (a), showing the relative position of the skyrmion center (the solid circles) and the trap center (the symbols '×') at three different moments (A,B,C). (d) Trajectories of skyrmion center at different trap velocities. (e) The transient velocity of skyrmion.

3.2. Moving field trap

Furthermore, we find that the skyrmion can be dragged by a moving magnetic field trap which creates a radially gradient magnetic field. For that, we performed a series of simulations for the skyrmion driven by a moving trap along the x-axis direction with different velocities V_{trap}. The results are shown in figure 4, and supplemental movie I is available at stacks.iop.org/NJP/19/083008/mmedia. In these simulations, we assume that the magnetic field trap only acts on the region with a 30 nm radius (marked by the dotted circles) and the gradient strength is 0.15 mT nm^{-1}. The skyrmion center and the trapping center start from a same position. Due to the active area of the trap being much larger than the skyrmion size ($R_{SK} \sim 10$ nm), the skyrmion is completely captured by the trap at the initial moment. When the trap of the magnetic field gradient moves along the x-direction with $V_{trap} = 1.1$ m s^{-1}, the result shows that the skyrmion can be dragged perfectly but its trajectory behaves as a periodic motion of parabola curves, as shown in figure 4(a). To gain insight into this parabolic motion, figure 4(b) shows the relative position between the skyrmion and the magnetic field trap center at three different moments (A, B, and C). In the beginning (moment 'A'), the skyrmion is behind the trap because v_x smaller than V_{trap}. But the skyrmion speed (i.e. the norm of its velocity vector, $v = \sqrt{v_x^2 + v_y^2} = 1.5$ m s^{-1}) is larger than that of the trap. Due to the spiral motion of the skyrmion driven by a radially gradient fields, the v_x of skyrmion in region II of figure 3(a) is enhanced. As a result, the skyrmion is accelerated in the x-direction and catches up with the trap somewhere between A and B. After this, the skyrmion is located in region I of figure 3(a), and v_x will decrease. Thus, the moving trap will catch up and pass the skyrmion again, see moment 'C' in figure 4(b). Consequently, the skyrmion follows the periodic motion of a parabolic curve, as shown in figure 4(a) and supplemental movie I.

However, when the magnetic field trap speed is increased to 1.5 m s^{-1}, the skyrmion cannot catch up with the trap and it will stop somewhere, as shown in figure 4(c). In this case, the approach using the moving magnetic field trap to control skyrmion motion will be invalid. Figures 4(d) and (e) summarize the trajectories and the

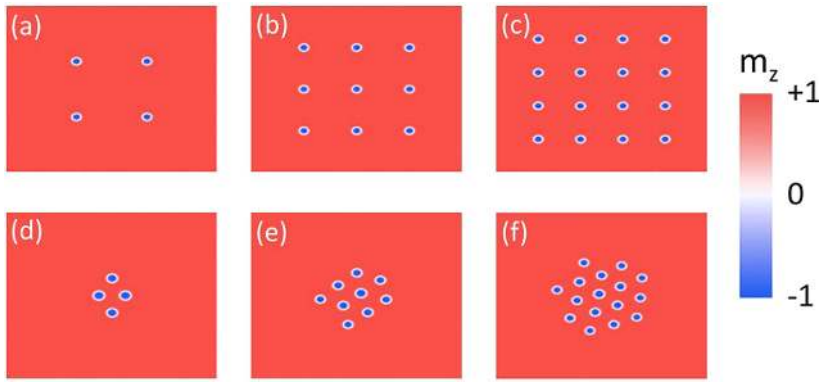

Figure 5. Capture of multiple skyrmions by a circular magnetic field gradient. (a)–(c) show the initial state of skyrmion array. (d)–(f) show the stable state obtained after some time.

transient moving velocity of the skyrmion center at different speeds of the trap, showing that a critical speed of the moving trap to drag the skyrmion persistently exists at $V_{\text{trap}} \sim 1.2$ m s^{-1}.

4. Trapping multiple skyrmions

Figure 5 shows a series of skyrmions with different numbers of 2×2, 3×3, and 4×4 trapped by the radially gradient magnetic field. In this case, all skyrmions are propelled by the magnetic field gradient towards the center of the sample. Different from the case of an isolated skyrmion, a collision effect among the skyrmions will occur, but the particle-like skyrmions cannot be fused together due to the repulsive interaction between them. As a result, a stable hexagonal distribution is eventually formed for these skyrmions, see figures 5(a)–(f) [44]. The separation between two skyrmions is determined by the competition between the repulsive force and the driving force from the gradient field [45]. The supplemental movie II shows the trapping process of a group of 3×3 skyrmions.

Finally, we would like to point out that the trapping of magnetic skyrmions has attracted much attention recently. Different techniques have been proposed, for example, using a hole (defect effect) [42, 46, 47] or electric field gradient [30] to guide the skyrmion motion. Here we would like to point out that a radially gradient magnetic field may be generated by different experimental techniques, such as a magnetic tip or a magnetic dot deposited on top of a thin film. For example, for magnetic force microscopy, if the magnetic tip is made of CoCr material ($M_S = 80$ kA/m) with a size of $40 \times 40 \times 80$ nm^3, our calculation shows that a radial gradient of the magnetic field with maximum value of 0.5 mT nm^{-1} can be created (not shown), in which we assume that the separation between the tip and the sample surface is 20 nm. Obviously, this gradient field can be used to trap the skyrmions. In addition, the gradient magnetic field may also be created by a superconducting vortex system [48, 49] or circularly polarized laser technique [18, 32, 50, 51].

5. Conclusion

In summary, we have investigated the skyrmion motion triggered by a magnetic field gradient. The velocity of skyrmion motion is predicted analytically through the Thiele approach, which agrees well with micromagnetic simulations. The skyrmion velocity increases almost linearly with increased magnetic field gradient. The component of velocity along the x-axis direction is almost unchanged for the small Gilbert damping factor ($\alpha < 0.1$) while the y-component of the velocity slightly increases with the damping factor. More interesting is that we have demonstrated a potential approach for trapping skyrmions using a radially spatial gradient of magnetic fields. The skyrmions can also be dragged by a moving magnetic tip which is used to create a radially spatial gradient of magnetic fields.

Acknowledgments

This work is supported by the National Basic Research Program of China (2015CB921501) and the National Natural Science Foundation of China (Grant No. 51471118, No.11274241). YZ acknowledges support by the National Natural Science Foundation of China (Project No. 11574137) and Shenzhen Fundamental Research Fund under Grant No. JCYJ20160331164412545.

References

[1] Fert A, Cros V and Sampaio J 2013 *Nat. Nanotech.* **8** 152–6
[2] Nagaosa N and Tokura Y 2013 *Nat. Nanotech.* **8** 899–911
[3] Liu E *et al* 2016 *Appl. Phys. Lett.* **108** 132405
[4] Zhang X, Ezawa M and Zhou Y 2015 *Sci. Rep.* **5** 9400
[5] Yu X Z, Onose Y, Kanazawa N, Park J H, Han J H, Matsui Y, Nagaosa N and Tokura Y 2010 *Nature* **465** 901–4
[6] Khalili Amiri P, Alzate J G, Cai X Q and Ebrahimi F 2015 *IEEE Trans. Magn.* **51** 1–7
[7] Kittel C 1946 *Phys. Rev.* **70** 965–71
[8] Shinjo T, Okuno T, Hassdorf R, Shigeto K and Ono T 2000 *Science* **289** 930–2
[9] Liu Y, He H and Zhang Z 2007 *Appl. Phys. Lett.* **91** 242501–3
[10] Liu Y, Hou Z, Gliga S and Hertel R 2009 *Phys. Rev.* B **79** 104435
[11] Moutafis C, Komineas S and Bland J A C 2009 *Phys. Rev.* B **79** 224429
[12] Hagemeister J, Romming N, von Bergmann K, Vedmedenko E Y and Wiesendanger R 2015 *Nat. Commun.* **6** 8455
[13] Jiang W *et al* 2015 *Science* **349** 283–6
[14] Papanicolaou N and Zakrzewski W J 1996 *Phys. Lett.* A **210** 328–36
[15] Mühlbauer S, Binz B, Jonietz F, Pfleiderer C, Rosch A, Neubauer A, Georgii R and Böni P 2009 *Science* **323** 915–9
[16] Sun L, Cao R X, Miao B F, Feng Z, You B, Wu D, Zhang W, Hu A and Ding H F 2013 *Phys. Rev. Lett.* **110** 167201
[17] Zhou Y, Iacocca E, Awad A A, Dumas R K, Zhang F C, Braun H B and Akerman J 2015 *Nat. Commun.* **6** 8193
[18] Ezawa M 2010 *Phys. Rev. Lett.* **105** 197202
[19] Dzyaloshinsky I 1958 *J. Phys. Chem. Solids* **4** 241–55
[20] Moriya T 1960 *Phys. Rev.* **120** 91–8
[21] Zang J, Mostovoy M, Han J H and Nagaosa N 2011 *Phys. Rev. Lett.* **107** 136804
[22] Sampaio J, Cros V, Rohart S, Thiaville A and Fert A 2013 *Nat. Nanotech.* **8** 839–44
[23] Iwasaki J, Mochizuki M and Nagaosa N 2013 *Nat. Nanotech.* **8** 742–7
[24] Jonietz F *et al* 2010 *Science* **330** 1648–51
[25] Du H *et al* 2015 *Nat. Commun.* **6** 8504
[26] Zhou Y and Ezawa M 2014 *Nat. Commun.* **5** 4652
[27] Everschor K, Garst M, Binz B, Jonietz F, Mühlbauer S, Pfleiderer C and Rosch A 2012 *Phys. Rev.* B **86** 054432
[28] Purnama I, Gan W L, Wong D W and Lew W S 2015 *Sci. Rep.* **5** 10620
[29] Liu Y-H, Li Y-Q and Han J H 2013 *Phys. Rev.* B **87** 100402
[30] Upadhyaya P, Yu G, Amiri P K and Wang K L 2015 *Phys. Rev.* B **92** 134411
[31] Kong L and Zang J 2013 *Phys. Rev. Lett.* **111** 067203
[32] Koshibae W and Nagaosa N 2014 *Nat. Commun.* **5** 5148
[33] Schütte C, Iwasaki J, Rosch A and Nagaosa N 2014 *Phys. Rev.* B **90** 174434
[34] Oh Y-T, Lee H, Park J-H and Han J H 2015 *Phys. Rev.* B **91** 104435
[35] Zhang X, Ezawa M, Xiao D, Zhao G P, Liu Y and Zhou Y 2015 *Nanotechnology* **26** 225701
[36] Komineas S and Papanicolaou N 2015 *Phys. Rev.* B **92** 064412
[37] Gilbert T L 2004 *IEEE Trans. Magn.* **40** 3443–9
[38] Thiele A A 1973 *Phys. Rev. Lett.* **30** 230–3
[39] Schulz T, Ritz R, Bauer A, Halder M, Wagner M, Franz C, Pfleiderer C, Everschor K, Garst M and Rosch A 2012 *Nature Phys.* **8** 301–4
[40] Garcia-Sanchez F, Sampaio J, Reyren N, Cros V and Kim J V 2016 *New J. Phys.* **18** 075011
[41] Troncoso R E and Núñez A S 2014 *Phys. Rev.* B **89** 106–14
[42] Müller J and Rosch A 2015 *Phys. Rev.* B **91** 054410
[43] Vansteenkiste A, Leliaert J, Dvornik M, Helsen M, Garcia-Sanchez F and Van Waeyenberge B 2014 *AIP Adv.* **4** 107133
[44] Jan M 2017 *New J. Phys.* **19** 025002
[45] Zhang X, Zhao G P, Fangohr H, Liu J P, Xia W X, Xia J and Morvan F J 2015 *Sci. Rep.* **5** 7643
[46] Sani S, Persson J, Mohseni S M, Pogoryelov Y, Muduli P K, Eklund A, Malm G, Käll M, Dmitriev A and Åkerman J 2013 *Nat. Commun.* **4** 2731
[47] Hanneken C, Kubetzka A, Bergmann K V and Wiesendanger R 2016 *New J. Phys.* **18** 055009
[48] Pogoryelov Y, Muduli P K, Bonetti S, Mancoff F and Åkerman J 2011 *Appl. Phys. Lett.* **98** 192506
[49] Muduli P K, Heinonen O G and Åkerman J 2011 *J. Appl. Phys.* **110** 076102
[50] Vahaplar K *et al* 2012 *Phys. Rev.* B **85** 104402
[51] Finazzi M, Savoini M, Khorsand A R, Tsukamoto A, Itoh A, Duò L, Kirilyuk A, Rasing T and Ezawa M 2013 *Phys. Rev. Lett.* **110** 177205